RESEARCH ARTICLE

A Novel EMG-Based Variable Impedance Control Method for a Tele-Operation System Under an Unstructured Environment

JINGJING LI[1], GUIBIN LI[2], ZHEN CHEN[1], AND JIAN LI[1]

[1]Key Laboratory for Intelligent Control and Decision on Complex Systems, School of Automation, Beijing Institute of Technology, Beijing 100029, China
[2]Tianyiyun Technology Company Ltd., Beijing 100032, China

Corresponding author: Jian Li (yellowlightlee@163.com)

ABSTRACT In this paper, a novel variable impedance control method is proposed in bilateral tele-operation systems. Inspired by adaptability and stability of the human arm in unstructured environments, the varied parameters of the impedance state for the operator's arm are transferred to the slave robot to inherit the compliance profile of the human arm in this paper. Firstly, the impedance state of the arm is classified with the naïve Bayes classifier, based on the surface electromyogram signals measured by the MYO arm band. Secondly, during teleoperation tasks, the operator can intuitively regulate the impedance of the arm based on attributes of the remote environment with the help of a haptic device, and a variable impedance control scheme is employed. The target impedance parameters of the impedance controller can change in real time according to the received impedance information of the operator's arm, so as to realize the simulation of the compliance profile of the slave robot to the human arm, and make the system maintain different compliance in different environments. The comparative experiments, with fixed impedance parameters and variable impedance parameters, are carried out to verify the effectiveness and the feasibility of the proposed method. The experimental results show that the method proposed in this paper has higher flexibility and environmental adaptability than the fixed impedance teleoperation method.

INDEX TERMS Tele-operation, variable impedance control, stiffness estimation, surface electromyogram, naïve Bayes classification.

I. INTRODUCTION

In tele-operations such as plant decommissioning, astrospace exploration and remote surgery [1], the exchange between position instructions from the master side and the haptic feedback from the slave side allows an operator to realistically conduct complicated tasks through a slave robot in a remote environment [2].

However, a force-reflecting tele-operation control approach, which sends position instructions and receives haptic feedback from the slave side, cannot satisfy the compliance

The associate editor coordinating the review of this manuscript and approving it for publication was Laura Celentano.

profile of the operator [3]. For the slave robot, the conventional position or force control method cannot meet the demands of robotics tasks in various unstructured environments in terms of safety and flexibility. Furthermore, it has been discovered that motion stability of the human arm can be achieved by suitably adjusting the mechanical impedance, i.e., resistance to imposed motion, which is largely contributed by the spring-damper-like property of human muscles [2]. Hence, transferring the compliance profile of the operator's arm to the slave robot is a major concern in tele-robotics systems [4].

It is unavoidable to contact remote objects on the slave side of the tele-operation system. To guarantee safety and stability

when the slave-side robot interacts with the environment, impedance control, which can be described as a virtual mass-spring-damper model, should be considered [5], [6], [7]. However, the compliant performance cannot be ensured according to the impedance controller with fixed parameters [8]. Furthermore, an unstructured environment makes the performance even worse.

To enhance the capability of impedance control against these uncertainties, Seraji *et al.* modified the reference trajectory of the manipulator on the basis of stiffness estimation of the environment [6]. Unfortunately, in practical applications, exact values of stiffness of the environment in real time cannot be easily obtained. For different tele-operation tasks, the parameters of the impedance controller should be dynamically adjusted according to the characteristics of the external environment [9], [10], [11]. More naturally, transferring a human operator's compliance profile, which includes mechanical impedance to the slave robot, has attracted researchers' attention recently [12]. The operator at the master side can feel the contact force and trajectory of the slave robot and intuitively adjust the muscular activities of humans [13]. Once the compliance profile of the operator's arm changes, this profile is delivered to the impedance controller of the slave robot. In addition to position instructions, variable impedance control should be widely utilized for improving the flexibility of slave robots while completing tasks in unstructured environments [14].

To obtain the human intention force, the surface electro-myogram (sEMG) is widely employed as a controller input for robots, prosthetic devices and exoskeletons [15], [16]. Based on sEMG, impedance control in tele-operation was introduced to transfer human variable stiffness to the slave robot for more flexible operation [17]. Endpoint impedance adjustments can be regarded as internal force regulations exerted by groups of extensor and flexor muscles [18]. For instance, simultaneous increasing tension of the flexor and extensor muscles modifies the impedance at the joint and end-point levels of the human arm. The endpoint force fluctuation and impedance adjustment of the human arm were related to sEMG signals, which can be regarded as a linear mapping model for the stiffness of the human arm. Several studies have been conducted in recent years. M. Kim proposed a new regression strategy to enable continuous and proportional measurements and transmission of the grasping force by using sEMG signals in transient and steady states [19]. R. Meattini targeted a solution that mimicked the human ability to manage multi-finger grasping and finely modulated grasp impedance through pattern recognition of sEMG signals [20]. However, all these works lacked haptic feedback for the operator and reduced interaction safety and transparency to some degree [21]. Only position feedback is not sufficient for a tele-operated system to complete complicated and flexible tasks. Hence, interactive forces also need to be felt and regulated precisely in scenarios where robots will inevitably contact the external environment physically [22].

To estimate the compliance characteristics of the human arm, numerous techniques have been utilized. Ajoudani established a nonlinear model for muscular activities and took advantage of a linearization method to map EMG signals to the endpoint impedance of the human arm [23]. Yang designed an interface to transfer human impedance adaptive skill with sEMG signals, and achieved good performance [13]. It is hard to build an accurate model for mapping. Several regression algorithms have been researched [24] to estimate optimal linear and nonlinear regression models with artificial neural networks (ANN) [25], locally weighted projection regression (LWPR) [26], and other regression techniques [27]. These regression techniques provide satisfactory performance [19], and the estimated results of these techniques are continuous. It may deteriorate the compliant performance or even undermine system stability to simply use this estimated stiffness as the property of the virtual spring within the impedance model [28]. It is not practical to adjust only one parameter to change the impedance characteristics because the mass, damper and spring properties couple with each other [29].

This problem can be transformed into a classification problem, in which we can pre-tune the mass-damper-spring parameters to guarantee the stability of the tele-operation system. The naïve Bayes classification is a widely used tool for machine learning tasks where features of datasets are continuous [30]. There is no need to develop an accurate mapping model between sEMG signals and stiffness with the naïve Bayes classifier [31]. We also aim to improve the safety and flexibility of slave robots in various environments and to enhance tele-presence for operators. In our work, the slave robot works with impedance control under varied parameters.

There are two main contributions in the paper, which are listed as follows. Firstly, based on the sEMG signal, the NB classifier is used to identify and classify the different impedance states of the arm to visualize the arm strength. This method does not need to establish a mathematical model between the sEMG signal and the mechanical impedance, which can reduce the problem of reduced identification accuracy caused by inaccurate model. Secondly, during the teleoperation task, the slave robot can actively adjust the parameters of the impedance controller according to the impedance state of the operator's arm for different remote environments, so as to realize the simulation of the compliance characteristics of the robot to the arm, so that the slave robot can be externally better environmental adaptability and flexibility.

The rest of this paper is structured as follows. Section II presents the implementation of the proposed tele-operation system. Section III describes the problems that need to be addressed in this paper. An impedance control algorithm with variable parameters is introduced in detail, and the stability of the algorithm is demonstrated. In addition, the naive Bayes classifier, including feature extraction of sEMG signals and the design of the classifier, is introduced in this section. The experimental setup and results for the fixed impedance and the proposed variable impedance tele-operation system are

introduced in section IV. Finally, section V addresses the conclusions.

II. SYSTEM IMPLEMENTATION

In this section, the framework of the proposed tele-operation system is explained. As shown in Figure 1, there are haptic devices (Omega.6) and MYO armbands on the master side, while a UR3 robot arm with an F/T sensor serves as the slave manipulator. Omega.6 is employed as the master device in this system. The position of the end effector of Omega.6 can be read from the controller and converted into (X, Y, Z) coordinates, which are expressed in metric units. An MYO armband consists of 8 EMG electrodes that can detect muscle bio-electricity with a default sampling frequency of 200 Hz.

The human operator manipulates Omega.6 while sampling its endpoint coordinate. The coordinate is mapped to the workspace of the slave robot. The contact force between UR3 and the environment is detected by an F/T sensor. This signal serves as an input of the impedance controller to obtain trajectory deviations. Position instructions for the UR controller can be obtained by combining the mapped coordinate and trajectory deviation. Moreover, the operator can intuitively regulate the arm impedance state based on haptic feedback in the system. An MYO armband that can measure the muscular activities of the arm is worn on the operator's forearm. The impedance of the operator's arm can be estimated from the sEMG feature vector with the trained classifier. Furthermore, this estimated compliance profile is transferred to the slave robot to achieve more flexible and safer performance.
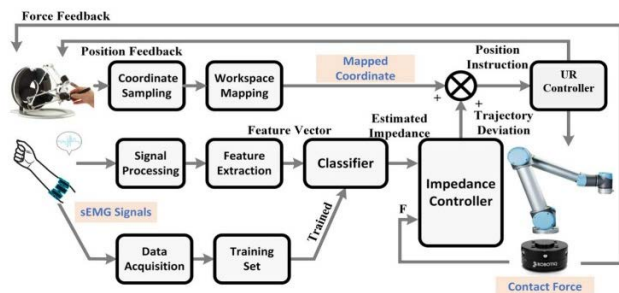

FIGURE 1. Tele-operation system with EMG-based human compliance profile transfer for impedance control with varied parameters.

In addition, preliminary works that include workspace mapping between Omega.6 and the UR3 robot, sample acquisition and feature extraction of sEMG signals are discussed as well.

A. WORKSPACE MAPPING

In contrast to Omega.6, which is based on parallel architecture, UR3 is a serial robot, and it is necessary to transform the coordinate system of the master device to the slave's. We take advantage of the linear transformation method summarized

in (1), which can map the master's workspace to the slave's.

$$\begin{bmatrix} x_s \\ y_s \\ z_s \end{bmatrix} = \begin{bmatrix} k_x & 0 & 0 \\ 0 & k_y & 0 \\ 0 & 0 & k_z \end{bmatrix} \begin{bmatrix} x_m \\ y_m \\ z_m \end{bmatrix} + \begin{bmatrix} b_x \\ b_y \\ b_z \end{bmatrix} \quad (1)$$

where the subscript s represents the coordinates from the slave robot, the subscript m denotes the coordinate of the master device, k is the mapping coefficient and b denotes the offset. The Monte Carlo method is utilized to generate point clouds that contain every accessible cartesian position of the endpoint of Omega.6 and UR3 within the angle limitation of each joint [19]. After calculating the limit coordinate values along the x-y-z axes for the master and slave, respectively, parameters for workspace mapping are obtained as

$$diag \left\{ k_x \quad k_y \quad k_z \right\} = diag \left\{ 3.94 \quad 2.25 \quad 3.31 \right\}$$
$$diag \left\{ b_x \quad b_y \quad b_z \right\} = diag \left\{ 0.3165 \quad 0.35 \quad 0.3962 \right\} \quad (2)$$

Figure 2 shows the point cloud of workspace mapping (the red area is the workspace of the robot arm, and the blue area is the workspace of Omega.6). What we desire is that the two main workspace overlap with each other as much as possible and that the slave's workspace includes the master's, which can ensure that every position in the master's workspace has only one corresponding point in the slave's workspace [32].
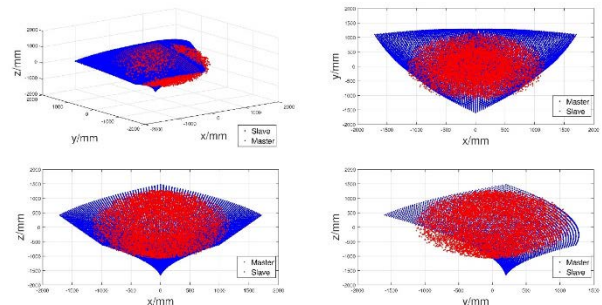

FIGURE 2. Workspace mapping.

B. DATA ACQUISITION

The relationship between the sEMG signals and the impedance of the human arm is not linear [23], which means it is not simple to develop a precise model to map the sEMG signals of 8 channels to the impedance. However, with the help of the machine learning method, it is not necessary to build a mapping model. The relationship can be obtained by the training set; furthermore, the impedance can be estimated by the trained relationship. Hence, it is crucial to collect the training set because it plays an important role in the classification performance. Figure 3 shows an image from the data acquisition experiments.

$$F_e = \begin{bmatrix} f_x & f_y & f_z \end{bmatrix}$$

An F/T sensor held in the hand of the human operator measures the grasp force along the x, y, and z directions. A pressure transducer is employed to measure the pressing
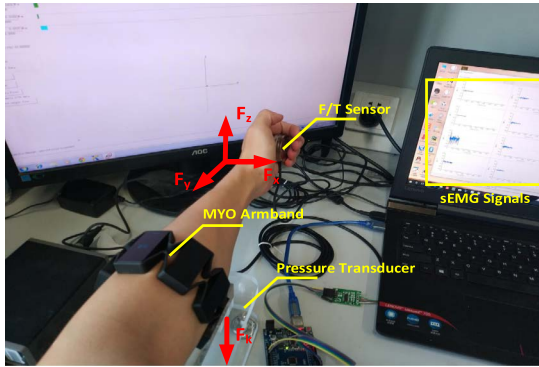
FIGURE 3. Data acquisition experiments.

force F_k of the arm. $F_e = [f_x \, f_y \, f_z]$ and F_k are the most directive indicators of stiffness of the human arm [2]. Hence, the label for one data sample can be obtained by the following:

$$c_i = \lceil \lambda F_e + \delta F_k \rceil \tag{3}$$

where c_i is the classification label for one sample and where λ and δ are weight factors.

C. FEATURE EXTRACTION OF sEMG SIGNALS
Since sEMG signals are significant, they can reveal the underlying patterns in impedance estimation. It is essential to filter out irrelevant information in sEMG signals and extract the key message for classification. The basic flow chart for sEMG signal processing is shown in Figure 4.

FIGURE 4. sEMG signal processing.

The process based on the sEMG signal mainly includes denoising of sEMG signals, feature extraction and classification. The sEMG signals provided by the MYO armband have already been preprocessed with an algorithm embedded in MYO. Therefore, this paper mainly focuses on feature extraction, which is employed for impedance estimation of the human arm. To recognize different states of impedance, it is necessary to extract features of sEMG signals under different impedance conditions. Classification mainly aims at matching the extracted features of raw signals [33].

Several different types of features of sEMG signals are used in this paper. They are listed as follows.

1) Absolute Mean Value (MAV): The MAV of sEMG signals reflects the intensity of muscle movements and the average intensity of the signals.

$$MAV = \frac{1}{N} \sum_{i=1}^{N} |x_i| \tag{4}$$

2) Root Mean Square (RMS): The RMS feature reflects a distribution of limb movement between muscles and the

muscle strength of each muscle group in the process of limb movement.

$$RMS = \sqrt{\frac{1}{N} \sum_{i=1}^{N} x_i^2} \tag{5}$$

3) Average Amplitude Change (AAC): The AAC reflects the fluctuation of the signal and can characterize the intensity of arm muscle activity

$$AAC = \frac{1}{N} \sum_{i=1}^{N} |x_{i+1} - x_i| \tag{6}$$

Each group of sample data can be transformed into a feature vector that consists of these three types of features extracted from raw sEMG signals in 8 channels. Feature vectors with a label are used to form the training set for training the classifier. During the tele-operation tasks, sEMG signals are sampled and transformed to a feature vector, which is used for classification in real time.

III. CONTROL STRATEGY
A. IMPEDANCE CONTROL
The impedance model is written as follows [34]:

$$M(\ddot{x} - \ddot{x}_d) + B(\dot{x} - \dot{x}_d) + K(x - x_d) = F \tag{7}$$

where M, B and K are inertia, damping and stiffness parameters of impedance control, respectively. x denotes the real trajectory, and x_d is the desired trajectory of the robot. Consider M, B and K as variables based on the mechanical state of the operators' arm in this paper. Let Δx represent $x_d - x$. The impedance control in this paper was inspired by [35]. F denotes the real contact force. The impedance control law is shown as

$$\begin{cases} K(t) = (k_p E_f + k_d \dot{E}_f + k_i \int_0^t E_f(\tau)d\tau)x_{dc}^{-1} + k_0 \\ M(t)\Delta\ddot{x} + B(t)\Delta\dot{x} + K(t)\Delta x = F \\ x_d = x_0 - \eta\Delta x \end{cases} \tag{8}$$

where k_0 and x_0 denote the modified stiffness and the initial position for the tele-operation tasks, respectively. E_f is the force tracking error, which is defined by $E_f = F_{ref} - F$, where F_{ref} is the reference force, and k_p, k_d, and k_i are the proportional, derivative and integral control gains, respectively. η is the coefficient used to reflect that the trajectory may change due to the unstructured environment.

The control law consists of variable parameters as well as a reference position correction, and the target stiffness can be adapted by a PID controller with the force tracking error [36]. Let the parameters in (8) be defined by the impedance state of the operator's arm. (7) becomes

$$M(t)\Delta\ddot{x} + B(t)\Delta\dot{x} + k(t)\Delta x = F$$
$$= F_{ref} - (1 + k_p)E_f - k_d\dot{E}_f - k_i \int_0^t E_f(\tau)d\tau \tag{9}$$

Since $\Delta x = x_d - x = x_0 - \eta \Delta x - x$ and the initial reference position x_0 is constant, the first-order and second-order derivatives of the trajectory correction are given by

$$\Delta \dot{x} = -\frac{\dot{x}}{1+\eta} \quad and \quad \Delta \ddot{x} = -\frac{\ddot{x}}{1+\eta} \quad (10)$$

Substituting (10) into (9) provides

$$M(t)\ddot{x} + B(t)\dot{x} + k_0 x - k_0 x_0 + (1+\eta)F_{ref}$$
$$= (1+\eta)\left\{(1+k_p)E_f + k_d \dot{E}_f + k_i \int_0^t E_f(\tau)d\tau\right\} \quad (11)$$

For simplicity, assume that the slave robot works in a pure rigid environment, which means F can be expressed by $F = k_e(x - x_e)$, where k_e takes different values at different stages and indicates the unknown stiffness of the environment; x and x_e are the trajectories of the robot and environment, respectively. As a result, the force tracking error can be written as

$$E_f = F_{ref} - F = F_{ref} - k_e(x - x_e) \quad (12)$$

Here, (12) implies that the real trajectory of the end effector of the robot can be approximated by

$$x = x_e + \frac{F_{ref} - E_f}{k_e} \quad (13)$$

Note that the trajectory x_e and stiffness k_e of environment are unknown and that x_e is variable so that $\ddot{x}_e \neq 0$ and $\dot{x}_e \neq 0$ Hence, we can obtain:

$$\dot{x} = \dot{x}_e + \frac{\dot{F}_{ref} - \dot{E}_f}{k_e} \quad and \quad \ddot{x} = \ddot{x}_e + \frac{\ddot{F}_{ref} - \ddot{E}_f}{k_e} \quad (14)$$

Substitute (14) into (11), and consider δx, which denotes the position tracking error of the inner-loop controller.

$$M(t)(\ddot{x}_e + \frac{\ddot{F}_{ref} - \ddot{E}_f}{k_e} + \delta \ddot{x}) + B(t)(\dot{x}_e + \frac{\dot{F}_{ref} - \dot{E}_f}{k_e} + \delta \dot{x})$$
$$+ k_0(x_e + \frac{F_{ref} - E_f}{k_e} + \delta x) = (1+\eta)\{(1+k_p)E_f$$
$$+ k_d \dot{E}_f + k_i \int_0^t E_f(\tau)d\tau\} + k_0 x_0 - (1-\eta)F_{ref} \quad (15)$$

Supposing that the first- and second-order derivatives of the position error of the inner-loop controller are smaller than those of the trajectory of the environment, define $\bar{x}_e$ by $\bar{x}_e = x_e + \delta x$, which enables the controller to address both the varying trajectory of the environment and the undesired position tracking error simultaneously. Equation (15) becomes (16) by substituting $\bar{x}_e$.

$$M(t)\ddot{\bar{x}}_e + B(t)\dot{\bar{x}}_e + k_0 \bar{x}_e + \frac{1}{k_e}[M(t)\ddot{F}_{ref} + B(t)\dot{F}_{ref}$$
$$+ (k_0 + k_e + \eta k_e)F_{ref}] = \frac{1}{k_e}(M(t)\ddot{E}_f + B(t)\dot{E}_f + k_0 E_f)$$
$$+ (1+\eta)\{(1+k_p)E_f + k_d \dot{E}_f + k_i \int_0^t E_f(\tau)d\tau\} + k_0 x_0 \quad (16)$$

Taking the Laplace transforms of the trajectory of the environment, the position error, force tracking error, initial reference trajectory and reference force can be rewritten as $L\{\bar{x}_e\} = X_e(s), L\{E_f\} = E_f(s), L\{X_0\} = X_0(s)$ and $L\{F_{ref}\} = F_{ref}(s)$, respectively. Equation (16) can be rewritten with the Laplace form.

$$(Ms^2 + Bs + k_0)X_e(s) + \frac{1}{k_e}[Ms^2 + Bs + k_0(k_0 + k_e$$
$$+ \eta k_e)]F_{ref}(s) = \frac{1}{k_e}(Ms^2 + Bs + k_0)E_f(s)$$
$$+ k_0 X_0(s) + (1+\eta)(1 + k_p + k_d s + \frac{k_i}{s})E_f(s) \quad (17)$$

Rearranging each term in (17), (18) is obtained.

$$E_f(s) = \frac{k_e s(Ms^2 + Bs + k_0)}{\lambda(s)} X_e(s)$$
$$+ \frac{s[Ms^2 + Bs + (k_0 + k_e + \eta k_e)]}{\lambda(s)} F_{ref}(s)$$
$$- \frac{k_0 k_e s}{\lambda(s)} X_0(s) \quad (18)$$

where $\lambda(s)$ corresponds to the characteristic equation of the transfer function and $\lambda(s) = Ms^3 + a_0 s^2 + a_1 s + a_2$. In addition, $a_0 = B + k_e(1+\eta)k_d$, $a_1 = k_0 + k_e(1+k_p)(1+\eta)$, $a_2 = k_e(1+\eta)k_i$. The block diagram of the impedance control scheme is shown in Figure 5, where the real contact force is obtained by an F/T sensor mounted at the endpoint of UR3. Note that in the proposed impedance control scheme, the reference trajectory and the inertia, damping and stiffness parameters are simultaneously updated. These parameters change based on the impedance state of the operator's arm.
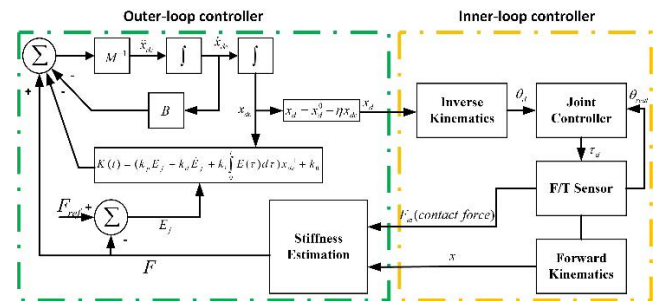

FIGURE 5. Block diagram of position-based impedance control.

B. STABILITY ANALYSIS

To analyse the stability condition for the proposed impedance control scheme, the Routh-Hurwitz array is constructed as follows.

s^3	1	a_1
s^2	a_0	a_2
s^1	$(a_0 a_1 - a_2)/a_0$	0
s^0	a_2	0

In the Routh-Hurwitz array, $a_0 > 0$, $a_2 > 0$, and $(a_0 a_1 - a_2)/a_0 > 0$ should be satisfied to guarantee the stability

of the proposed impedance control scheme. Noting that the proportional, derivative and integral control gains k_p, k_d, and k_i as well as the trajectory modification gain η are all positive, naturally the conditions $\alpha_i > 0$, $i = 0, 1, 2$ are ensured. Hence, expanding $a_0 a_1 - a_2 > 0$, we have

$$
\begin{aligned}
a_0 a_1 - a_2 &= (B + k_e(1+\eta)k_d) \times (k_0 + k_e(1+k_e)(1+\eta)) \\
&\quad - k_e(1+\eta)k_i > k_e(1+\eta)k_d \times k_e(1+k_p) \\
&\quad \times (1+\eta) - k_e(1+\eta)k_i = k_e^2(1+\eta)^2 \\
&\quad \times \{(1+k_p)k_d - \frac{k_i}{k_e(1+\eta)}\} > 0
\end{aligned}
\tag{19}
$$

If the environmental trajectory is considered to satisfy the unit step function, that is, $X_e(s) = 1/s$. Then for a fixed reference force $F_{ref}(s) = F_{ref}/s$, the force tracking error of the system in steady state E_f can be analyzed by the following formula.

$$
\begin{aligned}
\lim_{t \to \infty} E_f &= \lim_{s \to \infty} E_f(s) = \lim_{s \to \infty} s\{ \frac{k_e s(Ms^2 + Bs + k_0)}{\lambda(s)} \frac{1}{s} \\
&\quad + \frac{s[Ms^2 + Bs + (k_0 + k_e + \eta k_e)]}{\lambda(s)} \frac{F_{ref}}{s} \\
&\quad - \frac{k_0 k_e s}{\lambda(s)} \frac{x_0}{s} \} = 0
\end{aligned}
\tag{20}
$$

Based on the stability condition (19), six groups of parameters of M, B, k_0 that guarantee system stability can be tuned in advance. Different parameters would show different compliance performance [37]. Equation (20) shows that the proposed method can achieve that the force tracking error will not change abruptly even if the environment changes suddenly in the steady state. In addition, the parameters are determined by the compliance profile of the operator's arm. Hence, the impedance control scheme enables the robot to be adaptive to environmental changes in the steady state.

C. NAïVE BAYES CLASSIFICATION

The naive Bayes classifier is an efficient classifier in data mining [30]. This useful classifier is widely used in many applications, such as data stream classification. Naive Bayes is a generative model-based classifier [30] with fast learning and testing processes. Bayes' theorem is given as (21).

$$
p(c|y) = \frac{p(y, c)}{p(y)} = \frac{p(c)p(y|c)}{p(y)}
\tag{21}
$$

where c is the class label and y denote one sample. $p(c)$ is the prior probability, while $p(y|c)$ is the class-conditional probability. There are N possible class labels for each sample, and to minimize the overall conditional risk, we must select the class label that can maximize the posteriori probability $p(c|y)$. In such cases, our mission is to estimate human arm impedance as accurately as possible based on sEMG signals from eight tunnels. For every single sample y, the feature vectors extracted from the raw sEMG signals are all continuous; therefore, a Gaussian distribution should be applied as the a priori probability for better classification performance.

The naïve Bayes classifier is a simplified version of Bayesian classifiers that uses two assumptions. The former is that

the attributes of each sample are conditionally independent, and the latter is that there are no latent attribute effects on the label prediction process [30].

The vector $(y_1, \ldots, y_n|c)$ represents the n attributes of sample x. In this work, there are eight sEMG channels, and each channel has three attributes, so $n = 24$. The class-conditional probability of x can be computed by (22) and is supported by the above assumptions.

$$
p(y_1, \ldots, y_n|c) = \prod_{i=1}^{n} p(y_i|c)
\tag{22}
$$

To predict the class label of sample x, the probability of sample x in each class label is computed. The class with the maximum probability is identified as the class label of sample y. Equation (23) defines the label estimation process of sample x.

$$
C(y)_{NB} = \underset{c}{\arg\max}\, p(c) \prod_{i=1}^{n} p(y_i|c)
\tag{23}
$$

The Gaussian naïve Bayes classification is a special case of the naïve Bayes method with an assumption of a Gaussian distribution on attribute values. For example, suppose that the ith attribute is continuous and that its mean value and variance are represented by $\mu_{c,i}$ and $\sigma_{c,i}^2$, respectively. Hence, the probability of observing the value y_i in the ith attribute with the class label c is computed by (24), which is also called a normal distribution.

$$
p(y_i|c) = \frac{1}{\sqrt{2\pi\sigma_{c,i}^2}} e^{\left(-\frac{(y_i - \mu_{c,i})^2}{2\sigma_{c,i}^2}\right)}
\tag{24}
$$

where the mean value $\mu_{c,i}$ and variance $\sigma_{c,i}^2$ are obtained by (25).

$$
\begin{cases}
\hat{\mu}_c = \frac{1}{|D_c|} \sum_{y \in D_c} y \\
\hat{\sigma}_c^2 = \frac{1}{D_c} \sum_{y \in D_c} (y - \hat{\mu}_c)(y - \hat{\mu}_c)^T
\end{cases}
\tag{25}
$$

In this paper, we aim to complete multi-classification tasks to estimate six different impedance states of the human arm. The labels for these 6 classes are 0, 1, 2, 3, 4, 5, corresponding to the increasing impedance of the human arm.

IV. EXPERIMENTS AND RESULTS
A. EXPERIMENTAL SETUP
The experimental setup is shown in Figure 6. The UR3 robotic arm is employed as a slave robot with a Robotiq F/T sensor mounted at its end. Omega.6 serves as a haptic device on the master side, and the operator wears a MYO armband on the forearm that measures sEMG signals. The PC-side software communicates with the UR3 controller via Ethernet, and receives the sEMG signal measured by MYO via Bluetooth, which can display the operator's arm impedance state identification results and feedback information from the slave in real time.
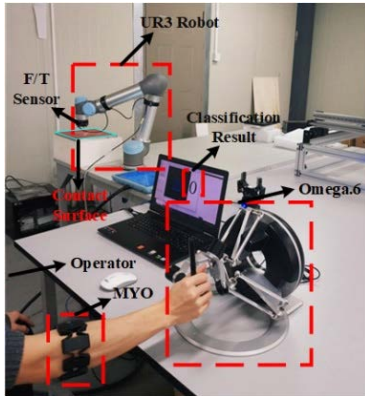
FIGURE 6. Experimental environment setup.

B. EXPERIMENTS

To verify the effectiveness of transferring the compliance profile of the human arm to the slave robot, a teleoperation comparison experiment of fixed impedance and variable impedance is carried out. The difference is that for different remote environments, the parameters of the variable impedance controller vary with the impedance state of the operator's arm, while the parameters of the fixed impedance controller are unchanged. The impedance state of the operator's arm is sampled and estimated through the MYO armband worn on the forearm.

In our experiments, six types of material with different attributes are employed to simulate different working environments for UR3. These materials include steel, rubber, hard plastics, hard Styrofoam, soft Styrofoam and sponge. These materials have different properties, especially in stiffness, and they range from very hard to soft. The experimental environment with different contact materials is shown in Figure 7.

FIGURE 7. Different materials employed in experiments.

The motion trajectory of UR3 follows instructions from Omega.6. Omega.6 is also capable of providing haptics based on force feedback measured by an F/T sensor. UR3 interacts with the outer environment, while the contact force and trajectories of the endpoint are sent back to the master side. The feedback force is not only the basis of haptic feedback for the operator but also the input for the impedance controller. Based on the contact force feedback from UR3, the positional deviation can be obtained by the position-based impedance controller. Motion instructions that combine coordinates of

Omega.6 and the position deviation are transferred to the UR3 robot controller through TCP transport.

As mentioned in Section III, the classifier is capable of distinguishing six impedance states of the operator's arm. Hence, at the pre-experiment stage, six groups of parameters were tuned for the impedance controller. All these parameters can guarantee the stability of the tele-operation system. In addition, the impedance parameters are variable and range between six groups of pre-tuned parameters in real time, and different parameters can make the robot exhibit different degrees of flexibility. The classification result determines which group of parameters to be employed in the impedance controller of the slave robot. For example, if the external environment is extremely hard, a very small displacement on the contact surface would produce a tremendous contact force between the slave robot and environment. Under this circumstance, it is necessary to instruct the robot to work very delicately for safety. In contrast, if the environment is very soft, the slave robot may need to work under very high stiffness for better performance. In this work, classification results are labelled with 0, 1, 2, 3, 4, 5. As the number increases, the parameters under a higher impedance are chosen.

At the beginning of each experiment, UR3 is tele-operated by the operator with Omega.6; hence, the trajectory of the slave device almost coincides with the trajectory of the master device. Then, the operator tele-operates UR3 to contact the environment gently. Once UR3 contacts the external environment, e.g., steel, rubber, hard plastics, hard Styrofoam, soft Styrofoam and sponge, the contact force is no longer zero and triggers the impedance controller. The controller outputs position deviations that combine with the endpoint coordinate of Omega.6 to provide motion instructions for UR3. During the fixed impedance experiments, the parameters in the impedance controller of the UR3 are all the same values in different remote environments. However, during the variable impedance experiments, the operator can evaluate the characteristics of the external environment and intuitively regulate the impedance of his/her arm according to the force feedback and position feedback of UR3. The impedance state of the arm can be classified with the trained classifier based on the sEMG signals measured by the MYO arm band. The classification result determines which group of parameters are employed in the impedance controller. Different classification results in different environments are shown in Figure 8.

The force and trajectories at both the master side and the slave side of fixed impedance and variable impedance are recorded in Figure 9 and Figure 10. All experiments focused on forces and trajectories along the z axis. In Figure 9 and Figure 10, F_s denotes the contact force at the slave side, and F_m is the force feedback at the master side. Z_m denotes the trajectory of the master device Omega.6 along the Z axis, while Z_s denotes the trajectory of UR3. $F_m = \Lambda F_s$, where Λ is the force feedback coefficient. The specific position deviations under impedance control with variable parameters are also shown in TABLE 1.
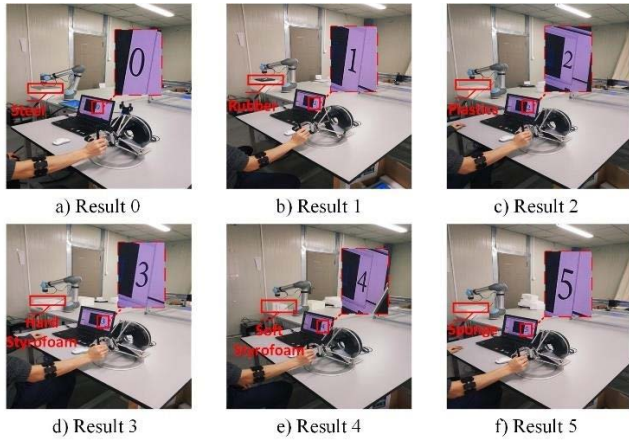
FIGURE 8. Classification results in different environments.

TABLE 1. Position deviations under impedance control.

position deviations	steel	rubber	hard plastics	hard Styrofoam	soft Styrofoam	sponge
Fixed parameters	0.1	0.12	0.12	0.13	0.11	0.1
Varied parameters	0.41	0.39	0.36	0.22	0.06	0.05
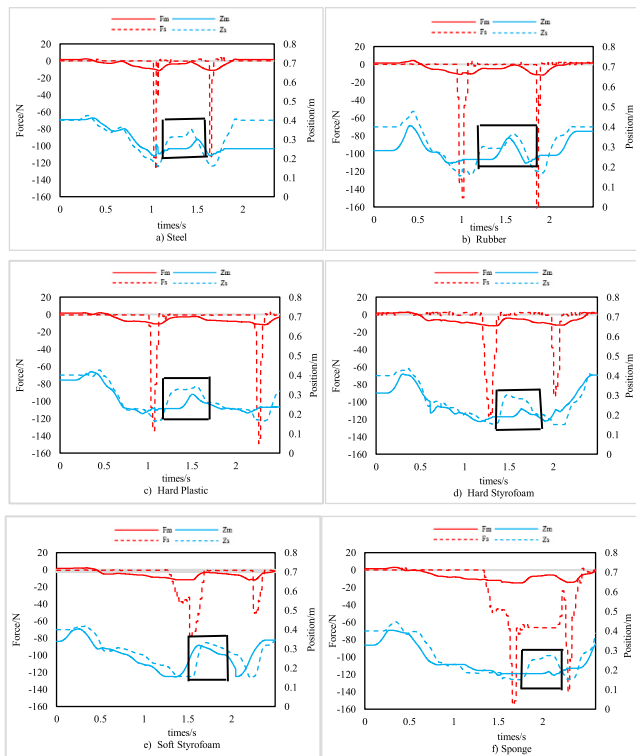
FIGURE 9. Force and trajectories under fixed parameters.

C. DATA ANALYSIS

In the experiments above, observing the Figure 9 and Table 1, it can be seen that the working performances of the UR3 with the fixed impedance method are almost the same
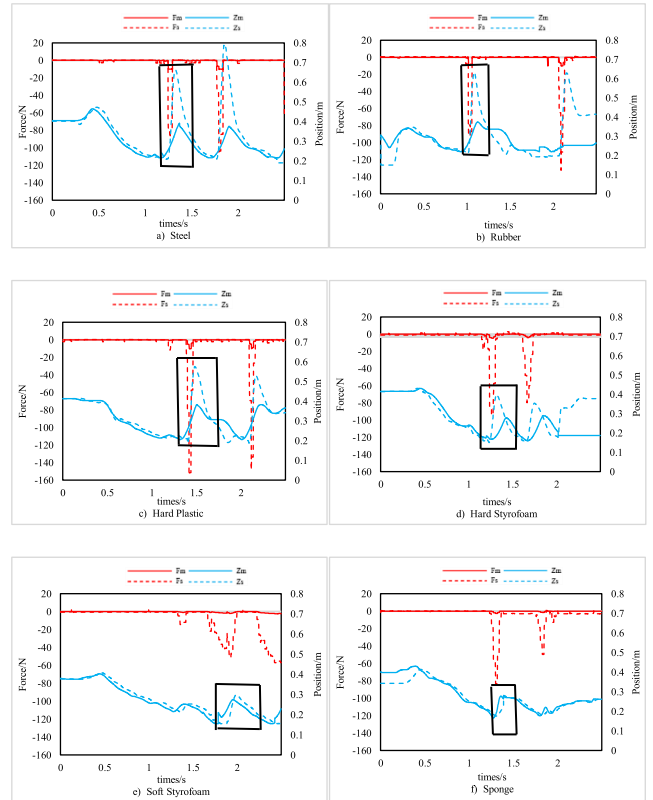
FIGURE 10. Force and trajectories under varied parameters.

regardless of the remote environment, and the corresponding positional deviations are similar. Meanwhile, through analyzing Figure 10 and Table 1, it can be seen that that the UR3 shows different flexibility for different remote environments and the corresponding positional deviations are also different under the variable impedance control method proposed in this paper.

Specifically, for variable impedance teleoparation experiments, if the environment is evaluated as a material with high stiffness, e.g., steel or rubber, the operator relaxes his/her muscles to make his/her arm fairly "soft". The state of the arm is estimated as "0" or "1" by the classifier. This compliance profile is transferred to UR3. From Figure 10 a), b), it is obvious that the contact force would cause large deviation outputs in the impedance controller because the slave robot shows flexible characteristics with low stiffness. There are tremendous deviations between Z_m and Z_s When F_s maintains 0, UR3 follows the instructions from Omega.6. As the stiffness of the external environment decreases, the impedance of UR3 is adjusted to be higher. Additionally, deviations between Z_m and Z_s decrease. For example, if UR3 interacts with quite soft materials, e.g., soft Styrofoam or sponge (in Figure. 10 e), f)), the impedance of the slave robot is rather high as if it is purely position-controlled. The deviations between the master trajectory and slave trajectory are quite small. Figure 10 c), d) shows the performance in the environment of hard plastics and hard

Styrofoam. It is obvious that the trajectory deviations are smaller than those under steel or rubber. According to the force and trajectories in different environments, the working performance of tele-operated robots with variable impedance control can be intuitively regulated by the operator. The sEMG-based compliance profile of the human arm is transferred to the slave robot. In addition, all the chosen parameters guarantee the stability and safety of the tele-operated system. In short, the variable impedance control method proposed in this paper has higher flexibility and environmental adaptability than the fixed impedance method.

V. CONCLUSION

In this paper, a compliant control method with variable parameters is proposed for the tele-operation system. With the impedance state classification of the human arm and impedance control with variable parameters for the slave robot, the proposed method enables the slave robot to show flexibility in an unstructured environment. The comparison experiments of fixed impedance and variable impedance have been carried out to verify the feasibility and effectiveness of the proposed method. The results show that impedance control with varied parameters shows better flexibility in an unstructured environment than impedance control with fixed parameters. Thus, it can be seen that the proposed varied parameters control method enables the slave robot to shows flexibility, and has the potential to complete complicated tasks in an unstructured environment.

In future works, we plan to introduce neuroadaptive control algorithms into the proposed method to obtain more detailed model information and improve the accuracy of impedance control. In addition, due to the close distance between master and slave, the influence of bilateral delay on the system is not considered in this paper. In the follow-up study, we plan to focus on a predictive control scheme to deal with the bilateral delay problem.

REFERENCES

[1] G. Gonzalez, M. Agarwal, M. V. Balakuntala, M. M. Rahman, U. Kaur, R. M. Voyles, V. Aggarwal, Y. Xue, and J. Wachs, "DESERTS: Delay-tolerant semi-autonomous robot teleoperation for surgery," in *Proc. IEEE Int. Conf. Robot. Automat. (ICRA)*, May 2021, pp. 12693–12700, doi: 10.1109/ICRA48506.2021.9561399.

[2] N. Wang, C. Yang, M. R. Lyu, and Z. Li, "An EMG enhanced impedance and force control framework for telerobot operation in space," in *Proc. IEEE Aerosp. Conf.*, Mar. 2014, pp. 1–10, doi: 10.1109/AERO.2014.6836500.

[3] P. K. Artemiadis and K. J. Kyriakopoulos, "EMG-based position and force control of a robot arm: Application to teleoperation and orthosis," in *Proc. IEEE/ASME Int. Conf. Adv. Intell. Mechatronics*, Sep. 2007, pp. 1–6, doi: 10.1109/AIM.2007.4412420.

[4] A. Dwivedi, D. Shieff, A. Turner, G. Gorjup, Y. Kwon, and M. Liarokapis, "A shared control framework for robotic telemanipulation combining electromyography based motion estimation and compliance control," in *Proc. IEEE Int. Conf. Robot. Automat. (ICRA)*, May 2021, pp. 9467–9473, doi: 10.1109/ICRA48506.2021.9560803.

[5] O. Khatib, "A unified approach for motion and force control of robot manipulators: The operational space formulation," *IEEE J. Robot. Autom.*, vol. RA-3, no. 1, pp. 43–53, Feb. 1987, doi: 10.1109/JRA.1987. 1087068.

[6] H. Seraji and R. Colbaugh, "Force tracking in impedance control," in *Proc. IEEE Int. Conf. Robot. Automat.*, vol. 2, Jun. 1993, pp. 499–506, doi: 10.1109/ROBOT.1993.291908.

[7] M. M. Rayguru, M. R. Elara, B. F. Gomez, and B. Ramalingam, "A time delay estimation based adaptive sliding mode strategy for hybrid impedance control," *IEEE Access*, vol. 8, pp. 155352–155361, 2020, doi: 10.1109/ACCESS.2020.3019429.

[8] Z. Song, Z. Wang, S. Guo, and B. Gao, "Study on resistance training for upper-limb rehabilitation using an exoskeleton device," in *Proc. IEEE Int. Conf. Mechatronics Automat.*, Aug. 2013, pp. 932–938, doi: 10.1109/ICMA.2013.6618040.

[9] Y. Kwon, A. Dwivedi, A. J. McDaid, and M. Liarokapis, "Electromyography-based decoding of dexterous, in-hand manipulation of objects: Comparing task execution in real world and virtual reality," *IEEE Access*, vol. 9, pp. 37297–37310, 2021, doi: 10.1109/ACCESS.2021. 3062364.

[10] E. Burdet, G. Ganesh, C. Yang, and A. Albu, "Interaction force, impedance and trajectory adaptation: By humans, for robots," in *Experimental Robotics* (Springer Tracts in Advanced Robotics), vol. 79, 2014, pp. 331–345, doi: 10.1007/978-3-642-28572-1_23.

[11] M. Gong and Y. Qin, "Research on the variable gain control strategy of tele-operation redundant robot," in *Proc. 8th Int. Conf. Intell. Hum.-Mach. Syst. Cybern. (IHMSC)*, Aug. 2016, pp. 408–411, doi: 10.1109/IHMSC.2016.41.

[12] X. Chen, N. Wang, H. Cheng, and C. Yang, "Neural learning enhanced variable admittance control for human–robot collaboration," *IEEE Access*, vol. 8, pp. 25727–25737, 2020, doi: 10.1109/ACCESS.2020.2969085.

[13] C. Yang, C. Zeng, P. Liang, Z. Li, R. Li, and C.-Y. Su, "Interface design of a physical human–robot interaction system for human impedance adaptive skill transfer," *IEEE Trans. Autom. Sci. Eng.*, vol. 15, no. 1, pp. 329–340, Jan. 2018, doi: 10.1109/TASE.2017.2743000.

[14] L. M. Doornebosch, D. A. Abbink, and L. Peternel, "Analysis of coupling effect in human-commanded stiffness during bilateral tele-impedance," *IEEE Trans. Robot.*, vol. 37, no. 4, pp. 1282–1297, Aug. 2021, doi: 10.1109/TRO.2020.3047064.

[15] R. Osu, D. W. Franklin, H. Kato, H. Gomi, K. Domen, T. Yoshioka, and M. Kawato, "Short- and long-term changes in joint co-contraction associated with motor learning as revealed from surface EMG," *J. Neurophysiology*, vol. 88, no. 2, pp. 991–1004, Aug. 2002, doi: 10.1152/jn.2002.88.2.991.

[16] Y. Xu, C. Yang, P. Liang, L. Zhao, and Z. Li, "Development of a hybrid motion capture method using MYO armband with application to teleoperation," in *Proc. IEEE Int. Conf. Mechatronics Automat.*, Aug. 2016, pp. 1179–1184, doi: 10.1109/ICMA.2016.7558729.

[17] G. R. Naik, S. E. Selvan, M. Gobbo, A. Acharyya, and H. T. Nguyen, "Principal component analysis applied to surface electromyography: A comprehensive review," *IEEE Access*, vol. 4, pp. 4025–4037, 2016, doi: 10.1109/ACCESS.2016.2593013.

[18] C. Yang, J. Luo, Y. Pan, Z. Liu, and C.-Y. Su, "Personalized variable gain control with tremor attenuation for robot teleoperation," *IEEE Trans. Syst., Man, Cybern. A, Syst.*, vol. 48, no. 10, pp. 1759–1770, Oct. 2018, doi: 10.1109/TSMC.2017.2694020.

[19] M. Kim, J. Lee, and K. Kim, "Tele-operation system with reliable grasping force estimation to compensate for the time-varying sEMG feature," in *Proc. IEEE Int. Conf. Robot. Automat. (ICRA)*, May 2016, pp. 5561–5567, doi: 10.1109/ICRA.2016.7487773.

[20] R. Meattini, S. Benatti, U. Scarcia, D. De Gregorio, L. Benini, and C. Melchiorri, "An sEMG-based human-robot interface for robotic hands using machine learning and synergies," *IEEE Trans. Compon., Packag., Manuf. Technol.*, vol. 8, no. 7, pp. 1149–1158, Jul. 2018, doi: 10.1109/TCPMT.2018.2799987.

[21] C. Yang, X. Wang, Z. Li, Y. Li, and C.-Y. Su, "Teleoperation control based on combination of wave variable and neural networks," *IEEE Trans. Syst., Man, Cybern., Syst.*, vol. 47, no. 8, pp. 2125–2136, Aug. 2017, doi: 10.1109/TSMC.2016.2615061.

[22] P. Kormushev, S. Calinon, and D. G. Caldwell, "Imitation learning of positional and force skills demonstrated via kinesthetic teaching and haptic input," *Adv. Robot.*, vol. 25, no. 5, pp. 581–603, 2011, doi: 10.1163/016918611X558261.

[23] A. Ajoudani, N. G. Tsagarakis, and A. Bicchi, "Tele-impedance: Towards transferring human impedance regulation skills to robots," in *Proc. IEEE Int. Conf. Robot. Automat.*, May 2012, pp. 382–388, doi: 10.1109/ICRA.2012.6224904.

[24] D. Yang, J. Zhao, Y. Gu, L. Jiang, and H. Liu, "EMG pattern recognition and grasping force estimation: Improvement to the myocontrol of multi-DOF prosthetic hands," in *Proc. IEEE/RSJ Int. Conf. Intell. Robots Syst.*, Oct. 2009, pp. 516–521, doi: 10.1109/IROS.2009.5354544.

[25] H. Srinivasan, S. Gupta, W. Sheng, and H. Chen, "Estimation of hand force from surface electromyography signals using artificial neural network," *Proc. 10th World Congr. Intell. Control Automat.*, Jul. 2012, pp. 584–589, doi: 10.1109-/WCICA.2012.6357947.

[26] C. Castellini and P. van der Smagt, "Surface EMG in advanced hand prosthetics," *Biol. Cybern.*, vol. 100, no. 1, pp. 35–47, 2009, doi: 10.1007/s00422-008-0278-1.

[27] A. Ziai and C. Menon, "Comparison of regression models for estimation of isometric wrist joint torques using surface electromyography," *J. Neuroeng. Rehabil.*, vol. 8, no. 1, p. 56, 2011, doi: 10.1186/1743-0003-8-56.

[28] X. Yang, C. Hua, J. Yan, and X. Guan, "An exact stability condition for bilateral teleoperation with delayed communication channel," *IEEE Trans. Syst., Man, Cybern., Syst.*, vol. 46, no. 3, pp. 434–439, Mar. 2016, doi: 10.1109/TSMC.2015.2444415.

[29] N. Hogan, "Impedance control: An approach to manipulation," in *Proc. Amer. Control Conf.*, vol. 1, Jun. 1984, pp. 304–313, doi: 10.23919/ACC.1984.4788393.

[30] L. Jiang, D. Wang, Z. Cai, and X. Yan, "Survey of improving naïve Bayes for classification," in *Proc. Int. Conf. Adv. Data Mining Appl.*, vol. 4632, 2007, pp. 134–145, doi: 10.1007/978-3-540-73871-8_14.

[31] B. Wang, C. Yang, and Q. Xie, "Human-machine interfaces based on EMG and Kinect applied to teleoperation of a mobile humanoid robot," in *Proc. 10th World Congr. Intell. Control Automat.*, Jul. 2012, pp. 3903–3908, doi: 10.1109/WCICA.2012.6359124.

[32] Z. Chen, S. Yan, M. Yuan, B. Yao, and J. Hu, "Modular development of master-slave asymmetric teleoperation systems with a novel workspace mapping algorithm," *IEEE Access*, vol. 6, pp. 15356–15364, 2018, doi: 10.1109/ACCESS.2018.2809860.

[33] J. Buzzi, G. Ferrigno, J. M. Jansma, and E. De Momi, "On the value of estimating human arm stiffness during virtual teleoperation with robotic manipulators," *Front Neurosci.*, vol. 11, p. 528, Sep. 2017, doi: 10.3389./fnins.2017.00528.

[34] C. Ott, R. Mukherjee, and Y. Nakamura, "A hybrid system framework for unified impedance and admittance control," *J. Intell. Robotic Syst.*, vol. 78, nos. 3–4, pp. 359–375, 2014, doi: -10.1007/s10846-014-0082-1.

[35] T. Kim, H. S. Kim, and J. Kim, "Position-based impedance control for force tracking of a wall-cleaning unit," *Int. J. Precis. Eng. Manuf.*, vol. 17, pp. 323–329, Mar. 2016, doi: 10.1007/s12541-016-0040-x.

[36] J.-H. Ryu, D.-S. Kwon, and B. Hannaford, "Stable teleoperation with time domain passivity control," in *Proc. IEEE Int. Conf. Robot. Automat.*, Apr. 2002, pp. 3260–3265, doi: 10.1109/ROBOT.2002.1013729.

[37] T. B. Sheridan, "Space teleoperation through time delay: Review and prognosis," *IEEE Trans. Robot. Autom.*, vol. 9, no. 5, pp. 592–606, Oct. 1993, doi: 10.1109/70.258052.

JINGJING LI received the B.E. degree in thermal energy and power engineering from Yantai University, Yantai, Shandong, China, in 2013, and the master's degree in control theory and control engineering from Yunnan University, Kunming, Yunnan, China, in 2016. She is currently pursuing the Ph.D. degree with the Beijing Institute of Technology, Beijing, China.

Her research interests include teleoperation, machine learning, human–robot interaction, and rehabilitation robots.

GUIBIN LI received the B.E. and master's degrees in electrical engineering and automation from the Beijing Institute of Technology, Beijing, China, in 2016 and 2019, respectively.

He has been an Engineer at Tianyiyun Technology Company Ltd., since 2019. His research interests include robotics, teleoperation, high-precision servo systems, and predictive control.

ZHEN CHEN received the master's degree in pattern recognition and intelligent systems and the Ph.D. degree in control theory and control engineering from the Beijing Institute of Technology, Beijing, China, in 2005 and 2008, respectively.

He is currently a Professor with the School of Automation, Beijing Institute of Technology. His research interests include spacecraft attitude maneuver control, robot control, electrical equipment, and space servo systems.

JIAN LI received the B.E. and master's degrees in mechanical engineering from Beijing Technology and Business University, Beijing, China, in 2006 and 2010, respectively, and the Ph.D. degree in mechanical engineering from the Beijing Institute of Technology, Beijing, in 2015.

He has been an Engineer with the School of Automation, Beijing Institute of Technology, since 2015. His research interests include modeling and design of robotics, high-precision servo systems, game theory control, and predictive control.

● ● ●